Keywords: methanol, spark ignition, medium speed, simulation, knock

Simulation of large bore methanol-fuelled spark ignition engines

Prof. Dr. ir. Sebastian Verhelst, Dr. ir. Ward Suijs, Dr. ir. Yi-Hao Pu

Ghent University

https://doi.org/10.18453/rosdok_id00004645

Abstract

Methanol is an appealing low or net zero carbon fuel. For large bore engines, most commercially available engines or engines close to being introduced to the market employ a dual-fuel approach. While this is attractive for quickly introducing methanol-capable engines, this comes with some disadvantages too. Methanol is by its nature more suitable to spark ignition (SI), but the SI concept – relying on flame propagation – is not easily applied to large bores and low speeds. This explains the lack of experimental data on large bore methanol-fuelled SI engines. The high knock resistance enabled by methanol, due to its high autoignition temperature, high charge cooling and high laminar burning velocity, means bore sizes could potentially be larger than for current high octane fuels. Moreover, the SI concept is attractive for its power density, cost and low emissions potential. Assessing the actual potential of a large bore methanol SI engine is most easily done through simulation, avoiding high upfront costs. However, due to the lack of data, the validation of simulation results is not straightforward. The paper explains the sub-models that were selected and refined, and the approach taken to get to trustworthy results. It discusses a methanol evaporation model for port fuel injection, approaches to obtain the burn rate for methanol SI combustion, and predicting the occurrence of knocking combustion. Integrating these sub-models into overall engine cycle simulations finally leads to some case studies that are discussed.

1. Introduction

Renewable fuels complement electrification, particularly for the heavy duty applications with high demands on power and autonomy. Methanol is a particularly interesting option as it can be produced in different ways, both from biomass as through the e-fuel route [1], or hybrids thereof [2]. Its unique proposition is that of being the simplest hydrogen carrier that is liquid at atmospheric conditions.

So far, renewable methanol has primarily been demonstrated for marine applications, in bore sizes going from truck-derived marine engines to large bore two-stroke engines. With some exceptions, these employ the dual-fuel principle, with a pilot injection of a high reactivity fuel (mostly diesel). This is done for several reasons. The main technical reason is the high autoignition temperature of methanol, preventing easy compression ignition (CI). A practical reason is the relatively straightforward retrofit of a diesel engine, through adding a port fuel injection (PFI) system for methanol. The ability of a dual fuel engine to switch to full diesel operation is also a compelling reason, offering redundancy and reducing the risk of being able to secure renewable methanol as its production is only just getting started.

Such dual fuel engines are characterized by their methanol energy fraction (MEF). The MEF is never 100%, due to the need for pilot fuel, and can drop down to 0% for the lowest and highest loads. The actual MEF depends on the engine technology and the application. For a PFI conversion, methanol will primarily burn in a flame propagation mode, with misfires limiting the achievable MEF at the lowest loads (due to excessively lean mixtures) and end-gas autoignition limiting the MEF at the highest loads. If the methanol can be directly injected, it can burn in a mixing-controlled fashion after being ignited by the pilot fuel burning. The high heat of vaporization, which we will come back to later, is then a limitation to the MEF at the lowest loads.

In the long run, it would be very attractive to be able to run engines fully on methanol. This would do away with the complexity of needing to bunker and store two fuels onboard, and could take full benefit from the fuel properties of methanol, such as the ability to completely eliminate soot formation as the carbon atom in the methanol molecule is bonded to an oxygen atom [3]. Although compression ignition operation on neat methanol has been demonstrated [4-6], methanol is more suited for a spark ignition (SI) concept, because of its high autoignition temperature.

SI concepts have traditionally been limited to relatively small bore sizes, for several reasons. Larger bores are needed for applications requiring higher power outputs, and for those applications the fuel cost is a large part of the total cost of ownership. Thus, high engine efficiency is desired. SI engines have both lower peak and part load efficiency than CI engines, the first because of compression ratio limitations resulting from the need to avoid end-gas autoignition (“knock”), the latter because of the pumping losses when throttling at part load.

Methanol’s fuel properties offer pathways to increase part and peak load efficiency of SI engines however: it is much more knock-resistant than gasoline, owing to its higher autoignition temperature and its large cooling effect. Its heat of vaporization is roughly 3.5 times that of gasoline, and its heating value half that of gasoline (requiring larger fuel volumes to be injected), which results in a about a sevenfold increase in cooling effect [1]. As end-gas autoignition is primarily a temperature-driven phenomenon, this greatly reduces the knock propensity. This has been known for over a century, with methanol or fuel blends containing methanol being used as racing fuel or aircraft piston engines using methanol or methanol-water blends as anti-knock agent [7,8]. Thus, higher compression ratios can be

employed, and/or optimal spark timing at high loads, benefiting peak efficiency. Part load efficiency on the other hand can be increased primarily due to the higher dilution tolerance of methanol, linked to its higher laminar burning velocity. This allows reducing pumping losses through either increased lean operation or increased amounts of exhaust gas recirculation (EGR).

There is, however, very limited data available on the potential efficiency of methanol SI operation [9], particularly for larger bore sizes [10]. Before investing in the testing of large bore SI engines on methanol, assessing the actually achievable bore sizes, power densities and efficiencies through numerical simulation is desired, which is the topic of this paper. The desired applications of the engine models were on the one hand, assessing whether a medium speed methanol engine using conventional spark ignition is possible; and on the other hand, for energy system optimization models (ESOMs). Such ESOMs model entire energy systems, for example at the level of a country, to shed light on the best strategies to reduce greenhouse gas emissions. Energy converters are part of such models, including combustion engines, but need to be strongly simplified, to the level of an efficiency number, or a scaling law relating fuel conversion efficiency to engine power [11]. Hence, the chosen approach was a 0D/1D one, as a compromise between computational expense and accuracy.

The main focus here, is how to model methanol's injection, evaporation and combustion (normal as well as abnormal, namely end-gas autoignition); the integration of these sub-models and the applications of the resulting complete engine model.

2. Simulation framework

Combustion in SI engines is characterized by flame front propagation. This premixed type of combustion can be modelled via a two-zone framework, distinguishing a burned and an unburned zone that are separated by a propagating flame front. The basic equations are derived from the conservation of energy applied to these two zones as follows,

$$\frac{d(m_u u_u)}{dt} = -p\frac{dV_u}{dt} - \frac{dQ_u}{dt} - \left(\frac{dm_{f,b}}{dt}h_f + \frac{dm_{a,b}}{dt}h_a\right) + \frac{dm_{f,i}}{dt}h_{f,i} \quad (1)$$

$$\frac{d(m_b u_b)}{dt} = -p\frac{dV_b}{dt} - \frac{dQ_b}{dt} + \left(\frac{dm_{f,b}}{dt}h_f + \frac{dm_{a,b}}{dt}h_a\right) \quad (2)$$

Here m denotes mass, u denotes internal energy, V denotes volume, Q denotes heat loss to the wall, and h denotes enthalpy. Subscript u denotes parameters pertaining to the unburned zone, b those for the burned zone, f denotes fuel, a denotes air, and i denotes injection. Note that the blow-by is neglected in Eqs. (1) and (2).

Eqs. (1) and (2) contain a term describing the burn rate. Different approaches can be taken to close these equations: either this burn rate can be prescribed, or it can be modelled. Both approaches are discussed in subsequent sections. Before covering the treatment of combustion, however, it is important to ensure that the conditions at the start of compression are correctly estimated. With port fuel injection of methanol, having a strong cooling effect (as explained above), an accurate model of methanol evaporation is needed. This is treated first.

2.1. Methanol evaporation model

Previous experience of the authors has learned that the high heat of vaporization of methanol can lead to problems getting methanol evaporated at the right time and the right place, so substantial effort was put into how to model this evaporation in a way that can be integrated in 0D/1D tools.

First, a simple experiment was set up to collect data on the evaporation of methanol in the intake runner of an engine, to guide the development of a suitable model. These measurements have been reported elsewhere [12]. Figure 1 depicts the overall concept of the proposed methanol evaporation model. The methanol spray is assumed to leave the injector nozzle in droplet form and then puddle at the inside of the intake runner as a thin layer of liquid film. Both droplets and liquid film are assumed to have a uniform temperature, and the proposed modelling framework deals mainly with the mass flux, ϕm, and heat flux, ϕq, at the liquid-gas interface, namely the surface of the droplet and the surface of the liquid film.

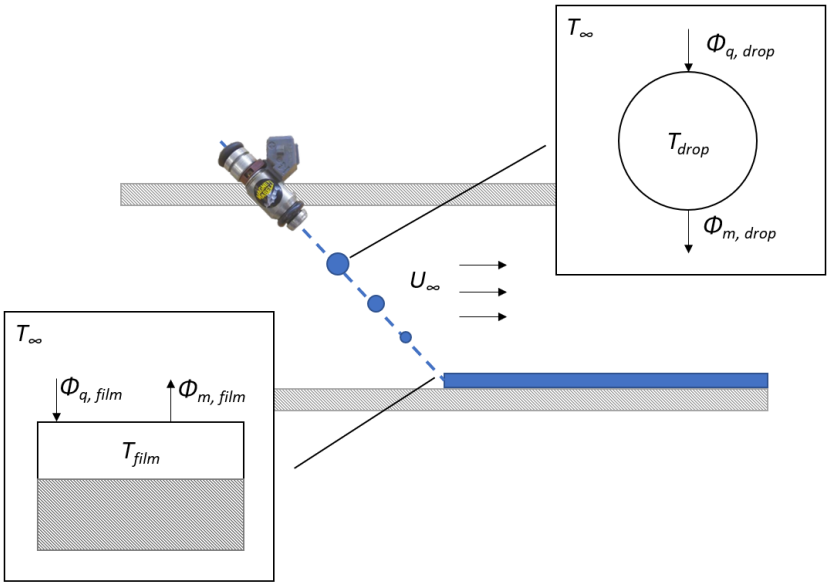

Figure 1: The schematic diagram of the proposed modelling framework in this research. Here, T is the temperature, U is the flow velocity, φ_m is the mass flux and φ_q is the heat flux. Subscripts 'drop' denotes the droplet, 'film' denotes the liquid film, and '∞' denotes the air flow.

For the droplet evaporation rate, the model proposed by Abramzon and Sirignano [13] is adopted due to its wide applicability and outstanding predictability compared to other models [14]. The instantaneous droplet evaporation rate is expressed in Eq. (3),

$$\dot{m}_{drop} = -2\pi R\rho D_{AB} Sh^* \ln(1 + B_M) \tag{3}$$

where R is the droplet radius, ρ is the air density, D_{AB} is the mass diffusivity of methanol vapour through air, Sh* is the modified Sherwood number that takes into account the Stefan flow and the thickness of a gas mixture film around each droplet.

The film evaporation rate is evaluated with Eq. (4) [15]

$$\dot{m}_{film} = A_{film}\phi_m = A_{film} M_{MeOH} k_c (c_{film} - c_\infty) \tag{4}$$

Where A_{film} is the surface area of the liquid film, k_c is the mass transfer coefficient, M_{MeOH} is the molar mass of the methanol, and c is the molar concentration of the methanol. Subscript *film* denotes the

concentration at the liquid film surface and ∞ denotes the concentration far away from the liquid film surface.

The temperature change of the air flow caused by both the droplet evaporation and the film evaporation can then be evaluated with Eq. (5)

$$\Delta T_{drop} = \frac{\dot{m}\Delta h_{vap}}{\dot{m}_{air} c_{p_{air}}} \tag{5}$$

Where $\dot{m}$ is the evaporation rate as either droplets or film, Δh_{vap} is the heat of vaporization of methanol, $\dot{m}_{air}$ is the air mass flow rate and $c_{p,air}$ is the specific heat capacity of air.

The thermophysical properties of air are referenced from [16] and the thermophysical properties of methanol are referenced from [17]. The viscosity and thermal conductivity of the mixture is calculated with the Wilke law [18].

The flow chart shown in Figure 2 summarizes the methodology for the proposed methanol evaporation modelling framework. To see the detailed calculation for each step, the readers are referred to [19].

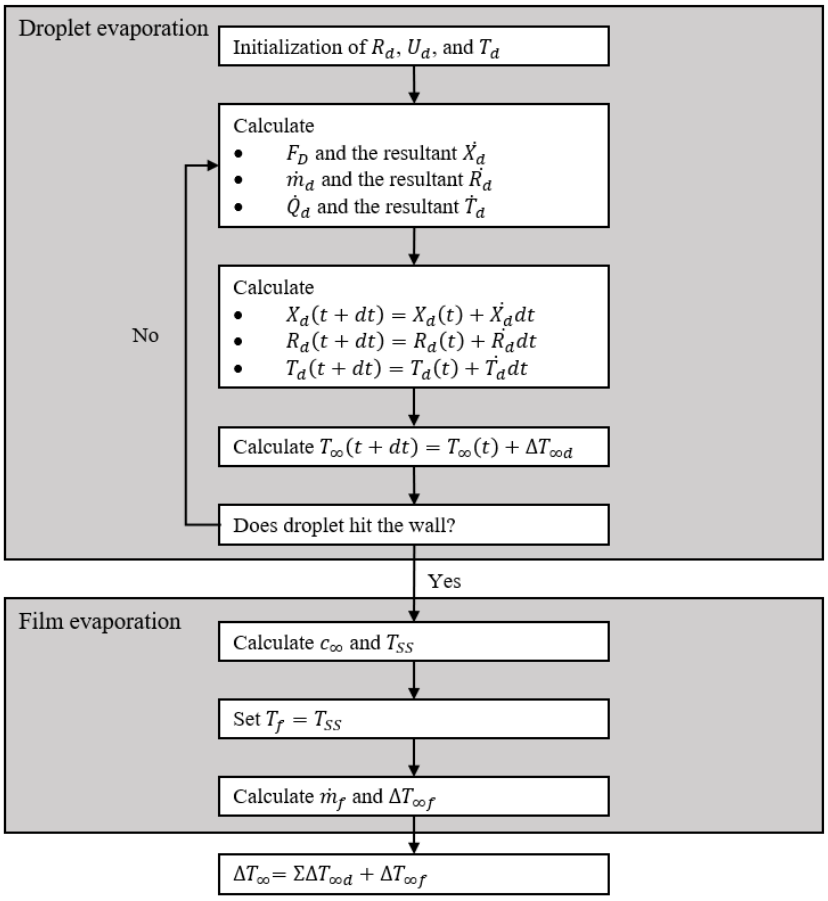

Figure 2: Flow chart of the proposed methodology to evaluate the temperature drop caused by methanol evaporation in the intake path.

One of the main conclusions of the model, that was validated using two sets of data from different engines employing port fuel injection [19], was that film evaporation is the dominant evaporation mode. Methanol droplets hardly get to evaporate before they impinge on the intake runner walls. On top of

this, if the intake is such that there is no room for a methanol film to form, only a very limited amount of methanol can evaporate before it enters the cylinders.

With the right conditions at the start of ignition, following the methanol evaporation, we now turn to the burn rate modelling.

2.2. Burn rate: prescribed

Two approaches were taken to determine the burn rate term, to close the two-zone pressure and temperature development equations. When studying the performance of end-gas autoignition prediction (Section 2.4), it was decided to impose a burn rate so as not to compound uncertainties in the burn rate prediction with those of the prediction of knocking combustion.

The available data on larger bore methanol SI engine operation was reviewed. The former combustion engine group at KTH Stockholm shared a comprehensive data set from a single cylinder version of a Scania D12 engine, converted to PFI SI operation with methanol, with a compression ratio of 13:1 [20]. The cylinder bore size was 127 mm, with a displacement of 1.95 liter. The dataset included sweeps of ignition timing, boost pressure and air-to-fuel equivalence ratios (lambda); all at 1200 rpm. A larger bore size and displacement volume was used at RWTH Aachen, with around 5 liter displacement, also using PFI [21].

From these data sets, Wiebe law parameters were extracted, as a function of lambda, see Table 1. These values were used in an initial estimation of the potential of a 256 mm bore PFI SI methanol-fuelled medium speed engine, see Section 3.1.

Table 1: Parameters of the Wiebe functions representing mass fraction burnt curves with different λ

Lambda	**1**	**1.5**	**2**
Combustion efficiency	98%	98%	98%
CA10-90 [°CA]	20	30	40
Wiebe exponent m	2	1	0.5

Rather than fixed values for certain lambdas, one can also try to capture the change in the burn rate curve in the form of a correlation. It was found that the KTH dataset could best be captured with a cosine law [22], where the combustion duration is predicted with the correlation of Alam et al. [23], which takes the compression ratio, spark timing, inlet pressure, lambda and engine speed into account. This approach was used for an assessment of the maximum bore of a methanol PFI SI engine, see Section 3.2.

2.3. Burn rate: predicted

The previous section used a data-driven approach, going from measured heat release profiles to burn rate profiles than can be imposed in a simulation. The section however also highlighted the lack of data on PFI SI methanol operation, particularly for larger bore sizes. An alternative approach is to predict the burn rate based on a turbulent burning velocity model, which typically requires the laminar burning velocity (LBV) as input. Specifically, the burn rate follows from the entrainment flame equations proposed by Blizard and Keck [24],

$$\frac{dm_e}{dt} = \rho_u A_e u_e \tag{6}$$

$$\frac{dm_b}{dt} = \frac{(m_e - m_b)}{\tau} \tag{7}$$

where me is the mass entrained by the flame front, ρ u is the density of the unburned mixture, A_e is the surface area of the flame front and u_e is the entrainment velocity. τ is a time constant that can be associated to λ_T, the Taylor length scale, and u_l, the laminar burning velocity (LBV), as expressed in Eq. (8):

$$\tau = \frac{\lambda_T}{S_l} \tag{8}$$

λ_T can then be associated to Λ, the integral length scale; Re_t the turbulent Reynolds number, and u′, the turbulent intensity as defined in Eqs. (9) and (10).

$$\lambda_T = C_{TLS} \frac{\Lambda}{\sqrt{R_{e_t}}} \tag{9}$$

$$R_{e_t} = \frac{\rho_u u' \Lambda}{\mu_u} \tag{10}$$

The form of the correlation that Metghalchi and Keck [25] originally proposed for the LBV was based on experimental data. This has been enhanced and modified by several other researchers. Vancoillie et al. [26] used a chemical kinetic code developed at Eindhoven University of Technology, CHEM1D [27], to compare different chemical kinetic mechanism of methanol oxidation against the published experimental data. Based on their studies, they selected the chemical reaction scheme of Li et al. [28] and calculated the LBV at different temperature (400-1000 K), pressure (5-105 bar), equivalence ratio (0.5-2) and EGR dilution ratio (0-50vol%). The calculation results were then used to establish an improved polynomial correlation. Mahendar and Erlandsson [29] have implemented this polynomial correlation in GT-POWER and demonstrated that it outperforms the default correlation within the software, especially when operating lean.

The major issue of the original correlation proposed by Vancoillie et al. [26] is that it is developed predominantly for automotive applications, hence the pressure range is not enough to cover the high in-cylinder pressure in HD engines. Similar to the method Suijs et al. [30] proposed for their knock/IDT model, Shahpouri et al. [31] calculated the LBV of methanol using the chemical reaction scheme from Pichler and Nilsson [32], with a much wider ranges of the input parameters compared to the work from Vancoillie et al., for example with the highest lambda going up to 4. All the dataset and codes from the work of Shahpouri et al. are made available online, including the artificial neural network (ANN) and support vector machine (SVM) models they trained for data retrieval. Since this research focuses on SI operation, the subset of the original dataset from Shahpouri et al. with excess air ratio up to 2 was extracted and used to train another ANN model with different hyperparameter as specified in Table 2. It can be noticed that with a much lower number of data points, the size of the trained ANN in this research can also be significantly smaller than the one from Shahpouri et al. Its predictions also agree better with the original calculation in terms of root mean square error (RMSE).

Table 2: Comparison of the hyperparameters and RMSE of ANN models from Shahpouri et al. and this research

	Shahpouri et al.	**This research**
Number of points	67518	23324
Number of hidden layers	2	4
Layer sizes	67, 266	10,10,10,5
Hidden Layer Transfer Function	Rectifier	tanh
Output Transfer Function	Rectifier	Sigmoid
RMSE [cm/s]	0.81	0.482

For the turbulent burning velocity (TBV), earlier work compared several models and concluded that the model proposed by Zimont fares well [33]. This was combined with a flame development model proposed by Lipatnikov and Chomiak [34]. A major concern after the attempt to calibrate the TBV models in the GT-Power environment is that it is unclear how thermophysical properties are evaluated within GT-POWER as the models fail to generate corresponding variations over a wide λ range. To avoid this issue, the thermophysical properties were estimated with data or correlations available in literature. However, the thermophysical properties of methanol in NIST [17] are only available up to 620 K. It was then decided to use the thermophysical properties of air to represent the air-methanol mixture in the cylinder. The term with the thermophysical properties that needs to be evaluated involves the Prandtl number and the mixture viscosity. This was found to be very close between air and air-methanol mixtures.

These two approaches: with a prescribed burn rate (with either a Wiebe or a cosine law, see Section 2.2) or a predictive burn rate model, were subsequently used together with a knock model, with the latter being the subject of the next section.

2.4. Knock model

With the equations listed above, a ”normal” premixed combustion event in SI engines can be modelled. SI engines can, however, also experience abnormal combustion. The specific abnormal combustion phenomenon that poses major operating constraints depends on multiple factors. End-gas autoignition, manifested as knock, is the largest concern for SI operation on methanol in large bore engines, thus it is important that the simulation tool is capable of predicting its occurrence. The phenomenological predictions of knock can be made based on the widely employed knock integral (KI) proposed by Livengood and Wu [35], as shown in Eq. (11),

$$KI = \int_{t_{IVC}}^{t_{KO}} \frac{dt}{\tau_{ID}(t)} = 1 \qquad (11)$$

where τ_{ID} is the instantaneous ignition delay time (IDT); t_{IVC} and t_{KO} are the time at the intake valve closure and knock onset respectively. The instantaneous IDT is defined as the delay from the moment an air-fuel mixture is exposed to certain conditions until it auto-ignites. The KI approach compares this characteristic time to the residence time of the unburned mixture in the cylinder to determine whether a knock event would occur or not. If KI reaches unity at a certain moment before exhaust valve open, knock is predicted to occur at that particular time. Otherwise, no knock is predicted.

By adopting this criterion, a knock model is in essence estimating the instantaneous IDT of various air-fuel mixtures exposed to various conditions. Suijs et al. [30] utilized a range of input parameters that are aligned with typical in-cylinder conditions of HD engines. The chemical kinetic software used was the open-source Cantera [36] and the reaction scheme used was also from Pichler and Nilsson [32] as it was found to give lower error under engine-like conditions. An ANN was trained with the tabulated IDT values for fast data retrieval.

3. Simulation results

The models described in the previous sections were used to investigate two research questions, linked to two research projects:

- Project FASTWATER [37] looked into, among many other things, whether a medium speed engine running spark ignition on port fuel injected methanol is feasible, i.e. what would be needed to ensure knock-free operation.
- Project BEST's [38] mission statement was to work out, for Belgium, the most economical electro- and synthetic energy carrier routes needed to face the climate change issues and ensure the stability of the grid and the security of supply in 2040 and beyond. As explained below, one of the pieces of the puzzle was to work out how large an engine running PFI SI on methanol can be, and how its power density and efficiency scales with engine size.

In order to do this, the models discussed previously were integrated either in a GT-Power environment, or in an in-house Matlab code (as specified below).

3.1. Case study: feasibility of knock-free operation of a PFI SI methanol-fuelled medium speed engine

First, a Wiebe law with the parameters as listed in Table 1 was used, along with a knock integral, to calculate to occurrence of knock on a medium speed engine with a 256 mm bore and 1000 rpm nominal speed. The results were reported elsewhere [39], and concluded that one needed to be able to ensure a 290 K intake temperature to allow the same power output as the baseline diesel engine, in order to avoid knocking operation.

The methanol evaporation model was used next to check the feasibility of attaining such an intake temperature. The temperature drop after introducing methanol in the intake path of the engine was evaluated using the methanol evaporation model. The injecting location was assumed to be the junction between the intake plenum and the individual runners that lead to the intake ports. The injection angle was assumed to be 45°. The geometries of the runner were referenced from the engine drawings.

The injector was assumed to be a commercially available product from Heinzmann GmbH, whose detailed information is published in [40]. According to it, the injection pressure was set to 10 bar and the initial droplet size is set to 0.175 mm.

Two different excess air ratios, corresponding to stoichiometric and lean operations, and 3 different boost levels, corresponding to 25%, 50%, and 75% of load on the original engine were used as the boundary conditions for the evaporation model. The results are detailed in Table 4.5. It can be seen that the lowest possible mixture temperature achieved is around 35.6 °C (= 308.8 K) which is far above the 290 K suggested by Pu et al. [39] to facilitate a knock-free operation with on-par output as the original diesel-fuelled DZC.

Table 3: The calculated temperature drops and methanol evaporated fractions under different operating conditions

Excess air ratio [λ]	**1**			**1.5**		
Boost pressure [abs. bar]	1.34	1.76	2.32	1.34	1.76	2.32
Intake air temperature	53.7	55.1	58.5	53.7	55.1	58.5
Evaporated fraction (Droplet)	1.3%	1.6%	2.1%	1.3%	1.6%	2.1%
Evaporated fraction (Film)	8.5%	7.5%	6.8%	12.9%	11.4%	10.4%
Evaporated fraction (Total)	9.8%	9.1%	8.8%	14.2%	13.0%	12.5%
Temperature drop (Droplet) [°C]	2.47	2.93	3.74	1.65	1.95	2.50
Temperature drop (Film) [°C]	15.61	13.72	12.40	15.81	13.93	12.68
Temperature drop (Total) [°C]	18.09	16.65	16.14	17.46	15.88	15.17
Mixture temperature [°C]	35.61	38.45	42.36	36.24	39.22	43.33

Further investigation reveals that a 290 K temperature after methanol injection is only possible if the initial droplet size (D_0) is reduced to 0.12 mm, which poses a significant challenge to the injector development under such a low injection pressure. Alternatively, the injection angle (θ inj) can be made smaller relative to the flow direction, which will ease the requirement of the D_0 to 0.145 mm.

The trajectories of the three different cases are illustrated in Figure 3, it can be seen that the high droplet evaporated fractions result from the extended airborne periods. However, if the intake runner is not long enough, eventually the droplets will land on the port walls or the back of the valve and the subsequent film evaporation will most likely not absorb heat from the air as these surfaces are hot.

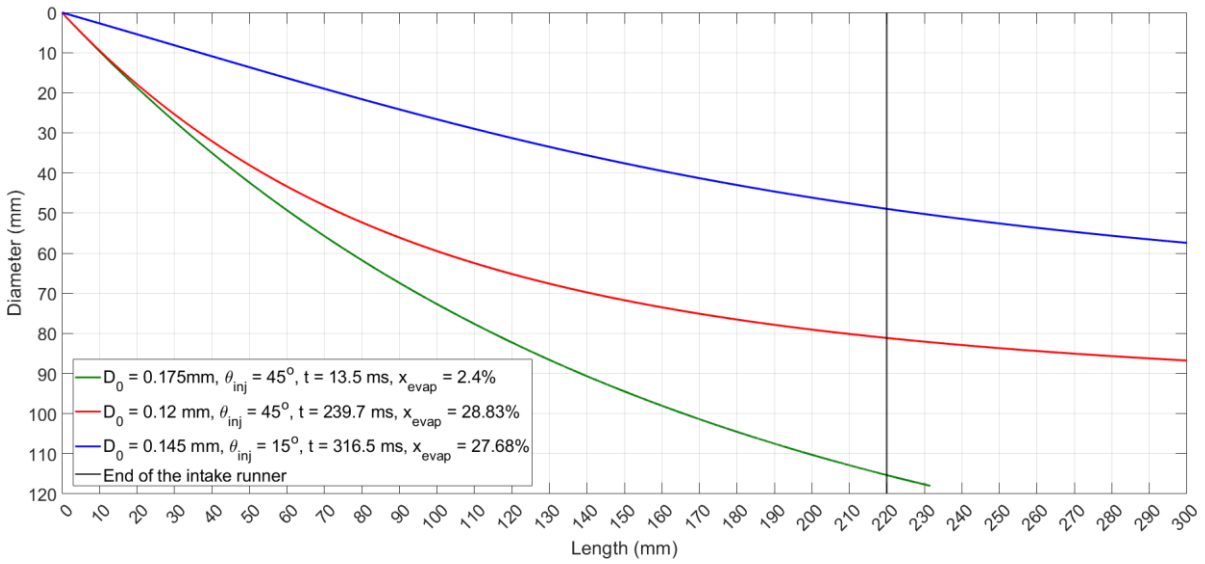

Figure 3: The droplet trajectories with different injection parameters. D_0 represents the initial droplet size, x_{evap} represents the evaporated fraction (as droplets), and ϑ_{inj} represents the injection angle relative to the intake air flow. The black line indicates the end of the intake runner, the droplets enter the cylinder head when they go beyond it.

The intake runner being too short is also the reason why film evaporation contributes so little to cooling down the mixture. There is simply not enough space in the intake runner to form a liquid film. Clearly, getting methanol evaporated in the intake is a challenging endeavour. The evaporation model is a helpful tool to explore potential solutions.

3.2. Scaling PFI SI methanol engines

With a predetermined and much-needed rise in renewable energy production, particularly solar and wind, a method of energy storage will be required to manage their intermittent nature. In addition, the applications that are difficult to electrify in the broad field of the mobility sector will have to part with their current use of fossil fuels. Within the BEST project, 'electrofuels' or 'e-fuels' are put forward as a possible solution to both issues. To create these fuels, renewable energy is combined with water to produce green hydrogen. This hydrogen can then be combined with nitrogen or carbon to produce a variety of fuels, which can be in either a liquid (e-methanol, e-gasoline, e-diesel) or gaseous (e-methane, e-ammonia) state at atmospheric conditions. Important questions that remain include how much e-fuels are needed to power the Belgian energy system and which technology is most efficient for converting these fuels back into final energy.

Given the variety of resources available, including nuclear, hydropower, wind and solar energy, as well as the existence of various conversion technologies, and the fluctuating demand and production, it is no longer feasible for an engineer to intuitively determine the optimal combination of these technologies for maximum economic efficiency. Therefore, multi-sector and whole-energy system optimisation models are being developed to assist in strategic energy planning of urban and regional energy systems. Due to the crucial role played by conversion technologies in these models, it is important to address their performance when running on the alternative e-fuels, particularly because these fuels can have significantly different properties than the conventional fossil fuels.

Here, the focus is on the internal combustion engine as energy converter. It is estimated that most of the light-duty applications where the ICE is currently used in, particularly passenger car applications, will be electrified as soon as possible and to the greatest extent possible. However, for heavy-duty applications such as long-haul trucks, marine propulsion, non-road mobile machinery, combined heat and power units and gensets, the low energy density of a battery electric drive will not be sufficient to meet autonomy requirements.

These applications are currently mainly powered by compression ignition diesel engines due to their high power output and efficiency. A research question here is if it would be possible to replace them with heavy-duty methanol-fuelled spark-ignition engines. As stated above, there are only a limited number of test cases to be found in the literature, which raises the question of what they are truly capable of. A two-zone semi-predictive zero-dimensional simulation model was developed within the commercial software MATLAB. The aim of this model is to predict the performance of methanol-fuelled port-fuel injected (PFI) SI engines as function of their size. A zero-dimensional approach was chosen over a quasi- or multidimensional approach due to the trade-off between accuracy and computational costs. The starting point for this model was a homogeneous two-zone finite heat release model featuring a constant combustion rate. It first did not include a heat transfer or knock model. Step by step, the complexity was increased by adding different sub-models to the simulation framework. To determine the optimal load point for each engine size, the burn rate had to respond to various imposed inlet operating conditions. As discussed in Section 2.2, burn rate parameters were experimentally derived from a heavy-duty Scania D12 PFI SI engine (B = 127 mm) and compared to

various correlations for the implementation of a semi-predictive combustion duration. Additionally, special attention has been given to the development of an improved Livengood & Wu knock model, as described in Section 2.4.

The two-zone model was subjected to an optimisation procedure to find the knock-limited operating load for each engine size. Different engine configurations were scaled based on the geometry of the Scania D12 engine (B = 127 mm), ranging from a bore size of 80 mm to 260 mm.

Each engine starts at low load and an optimisation process gradually increases the load until either the knock or peak pressure limit is reached. The following baseline starting conditions are set:

- An initial retarded spark timing of 10°ca aTDC
- In-cylinder pressure at IVC timing of 101.5 kPa (atmospheric conditions)
- n-cylinder temperature at IVC timing of 30 °C

The two-zone model then calculates the associated pressure and temperature trajectory of the burned and unburned gases and calculates the performance parameters, of which the achievable indicated mean effective pressure and indicated thermal efficiency are of main interest here. Simultaneously, the knock model evaluates the knock integral on a crank angle basis to check whether it exceeds one or not. From this point onwards, if knock is not occurring, spark timing is advanced by 1°ca increments until the CA50 reaches 10°ca aTDC or end-gas conditions increase to the point where knock occurs. Generally speaking, the spark timing where CA50 is between 8 - 10°ca aTDC is referred to as the minimum spark advance for maximum brake torque (MBT timing). This optimum timing is a compromise between starting combustion too early in the compression stroke and completing combustion too late in the expansion stroke [41]. If the spark timing can be advanced to this point without causing knock, it means that the engine load is below the maximum knock limit. Therefore, the charge density is then increased by increasing the intake pressure at IVC timing in 5 kPa increments. This step represents an increase in boost pressure to increase the load of the engine. To reduce the number of unknown variables, we furthermore assume that the in-cylinder temperature at IVC remains constant here regardless of the boost pressure.

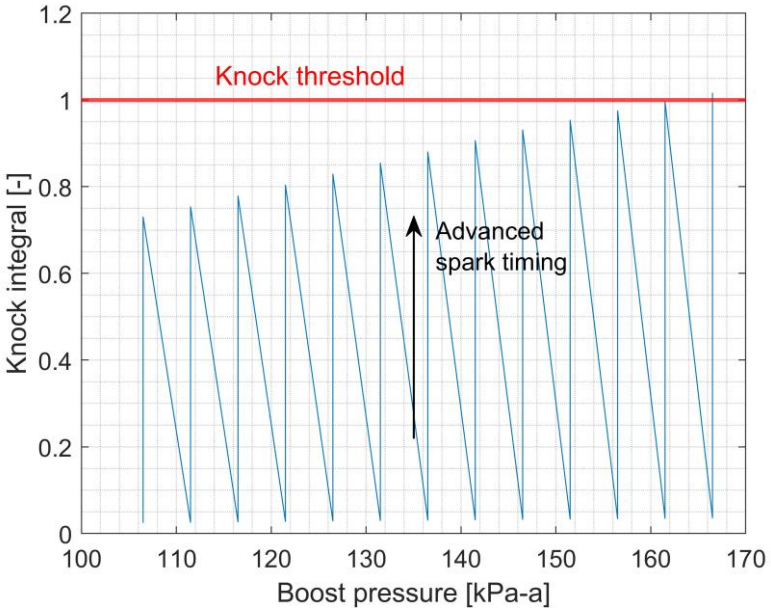

Figure 4: Illustration of the optimisation process for each engine configuration

Figure 4 illustrates the optimisation method. Starting from the left-hand corner, spark timing is advanced until CA50 reaches 10°ca aTDC. As the resulting knock integral value is less than one, the pressure can be increased to 105.5 kPa. This step is repeated until the knock integral reaches unity, in this example, at an inlet pressure of 165.5 kPa and a spark timing of -2°ca aTDC. The associated IMEP is called the knock-limited IMEP, and the parameter of interest for our upcoming scaling laws.

In addition, it is important to monitor the increase of load to ensure that it does not cause the peak pressure limit to be exceeded. At a constant inlet temperature, the higher intake pressure increases the charge density, causing the in-cylinder pressure to rise faster and to higher levels. Therefore, after each evaluation of the two-zone model, the optimisation procedure also compares the maximum in-cylinder pressure value with the defined limit.

An overview of the two-zone semi-predictive combustion model and its optimisation procedure is given in Figure 5. For each engine configuration, the initial operating conditions will be imposed, and the optimisation procedure will be executed to find the maximum indicated mean effective pressure and efficiency.

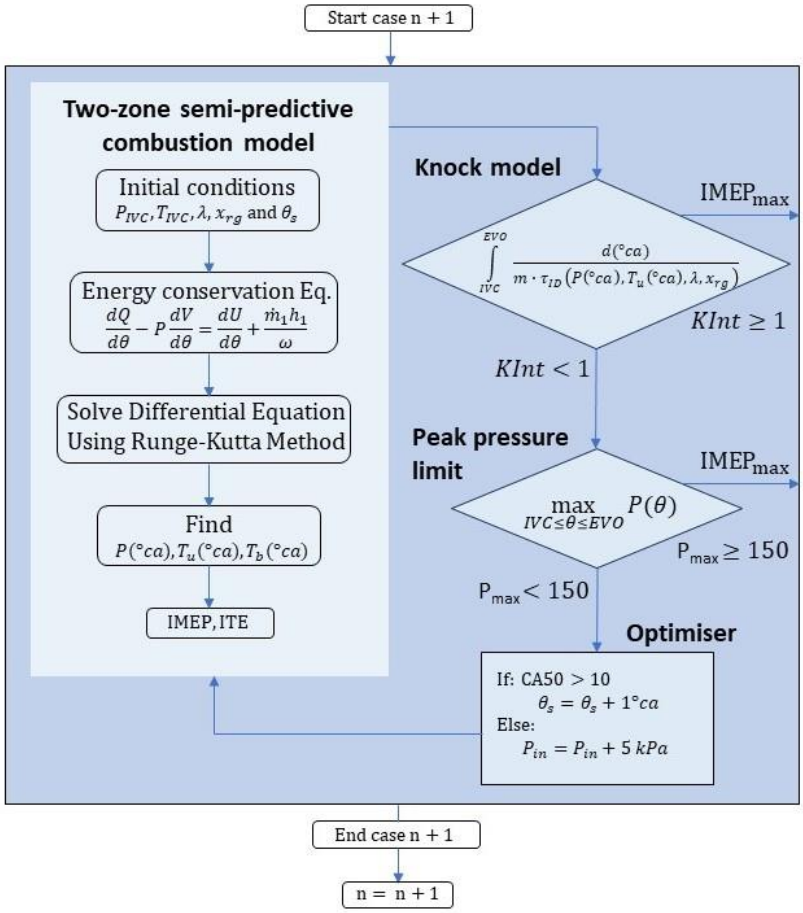

Figure 5: Flow chart of the optimisation procedure coupling a two-zone semi-predictive combustion model to a zero-dimensional knock model

The Scania D12 engine will be used as baseline engine for generating different (larger) engine geometries, as it is the only larger PFI SI methanol engine with a fairly comprehensive set of experimental data available [20].

To look at the performance of larger engines, the proportions of the combustion chamber are held constant; the stroke/bore ratio, connecting rod/stroke ratio and the compression ratio. However, engine rotational speed should not be considered as a constant. The speed of large-bore engines is limited by the inertial forces acting on the pistons. It was therefore decided to use a constant mean piston speed for each scaling law instead, as this parameter remains rather constant across different engine platforms. The engine's bore size was increased in increments of 10 mm, starting from 80 mm (automotive light-duty size) to 260 mm (medium speed engine size). Three mean piston speeds were investigated: the baseline value of 6.16 m/s (1200 rpm for the D12), as well as its double and triple values of 12.32 m/s and 18.54 m/s respectively. Starting with the lowest piston speed, engines up to a bore size of 110 mm are not limited by knock, but rather by the imposed peak in-cylinder pressure limit of the engine block. A near constant indicated mean effective pressure value of 29.6 bar corresponds to this pressure limit. For this range of engines, the thermodynamic limit has not yet been reached. Engine designers could therefore obtain even higher loads by investing in sturdier engine blocks. From 110 mm onwards, the IMEP becomes knock-limited. The main influence here will be the reduced rotational engine speed which decreases inversely with bore size for a constant stroke/bore ratio. The combustion duration (in seconds) will be increased, allowing the end-gases to have more

time to reach the conditions necessary to autoignite. For a bore size of 180 mm, the maximum IMEP will therefore only be 15 bar. For even bigger engine sizes, the trendline in Figure 6 stagnates. The reason for this is that boost pressure can no longer be applied without causing knock even for the latest spark timings, hence the model stops at ambient operating conditions and tries to advance the spark timing until the knock integral reaches unity.

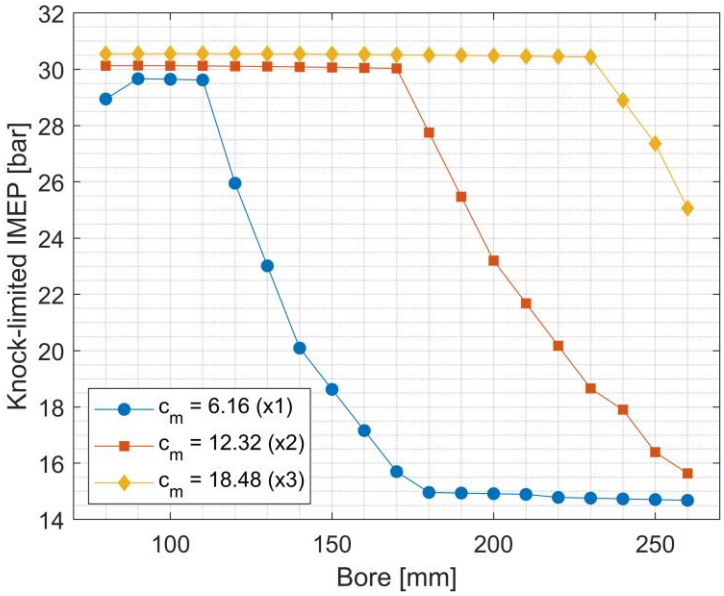

Figure 6: Knock-limited IMEP as function of bore size for different mean piston speeds and a fixed air-to-fuel ratio of lambda = 1

By doubling the mean piston speed (c_m = 12.32 m/s), the knock constraints are significantly lifted. Engines are now knock-free until a bore size of 170 mm. Using 25 bar IMEP as a target for heavy-duty diesel operation, PFI SI engines running on green methanol would therefore be a viable sustainable solution for engines up to 190 mm bore. For an even higher mean piston speed of 18.54 m/s, the engines are peak pressure limited up to 230 mm. Note however that such a mean piston speed value is already at the upper limit of what is possible in conventional spark-ignited engines [41]. Realistic performance values should therefore be sought between the first and second curve.

With respect to indicated thermal efficiency, the efficiency increases for higher mean piston speeds, see Figure 7. This is a result of the reduced residence time of the mixture in the cylinder, leaving less time for heat transfer to the surroundings. Note that if a friction model were added to predict the brake thermal efficiencies, the higher engine speed will have a detrimental effect due to the increased friction losses, hereby partially negating the previous effect. Looking at each curve individually, the efficiency for a c_m value of 6.16 m/s can be seen to drop in three stages. During the peak pressure limited stage, efficiency stays constant. The reduced surface area to volume ratio appears to have a negligible effect on efficiency improvement at larger bore sizes. After that stage, the IMEP becomes knock limited and efficiency reduces gradually together with the load. Once the inlet pressure reaches atmospheric conditions, the IMEP does not decrease significantly any more, however spark timing is retarded to remain below the knock limit. The efficiency therefore reduces as well. A similar behaviour can be seen for the higher mean piston speed curves, albeit to a much lesser extent due to the reduced occurrence of knock.

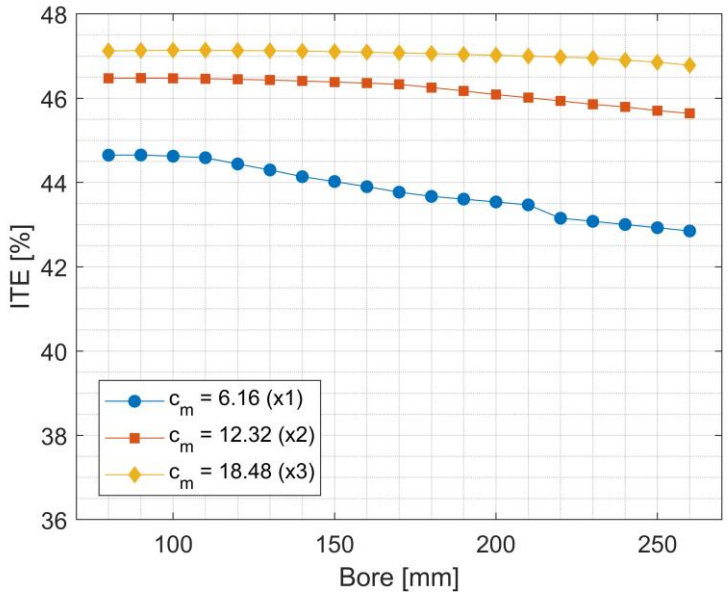

Figure 7: Indicated thermal efficiency as function of bore size for different mean piston speeds and a fixed air-to-fuel ratio of lambda = 1

The influence of the air-to-fuel ratio lambda on the knock-limited performance was investigated for the mean piston speed value of c_m = 12.32 m/s. Figure 8 shows the trend lines for lambda ranging from 1 to 1.6. For the same in-cylinder peak pressure limit of 150 bar, lower IMEP values are found in the pressure-limited zone. Due to the diluted mixture, a higher boost pressure is required to reach the same energy content in the cylinder. For lambda equal to 1.6, the maximum IMEP is 26 bar, while under stoichiometric conditions this could go up to 30 bar. On the other hand, the knock-limited zone is pushed further into larger bore engines. For lambda = 1.4, knock-limited operation only starts at 210 mm bore engines, while for lambda 1.6 it starts at 250 mm bore engines. At lean operating conditions, the ignition delay time becomes significantly larger, hereby postponing the moment of autoignition. In addition, because the loads are lower for the same boost pressure, the temperatures of the unburned gases are also reduced, which in turn increases again the ignition delay time. At the maximum bore size of 260 mm, the knock-limited IMEP is respectively 20.4 bar and 25.2 bar for lambda equal to 1.4 and 1.6. If an IMEP of 25 bar is targeted, PFI SI operation is possible up to 190 mm engines under stoichiometric operation. For leaner conditions, engines up to 230 mm and 260 mm are even feasible.

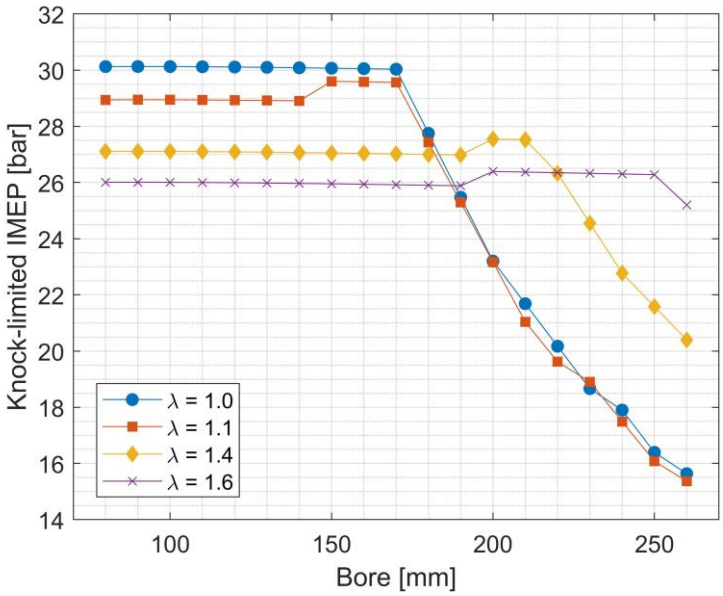

Figure 8: Knock-limited IMEP as function of bore size for different air-to-fuel ratios at a constant mean piston speed of c_m = 12.32 m/s

4. Conclusions

This paper reported work on important building blocks for 0D-1D simulation of PFI SI methanol engines:

- A methanol evaporation model, to allow the estimation of the evaporated fuel fraction in the intake. This is important to assess the temperature at the start of compression, which itself is crucial to determine the occurrence of end-gas autoignition and thus the achievable power density and efficiency of a methanol-fuelled PFI SI engine.
- The burn rate: data was extracted from the few reported measurements from literature, to fit either Wiebe law parameters or a cosine law, in order to be able to impose a burn rate in an engine simulation. Alternatively, one can opt for a predictive burn rate model, for which the laminar burning velocity (LBV) is an important input. A neural network was fitted to LBV calculations from chemical kinetics. The burn rate then results from an entrainment frame-work with appropriate models for the turbulent burning velocity and flame development.
- The occurrence of knock follows the Livengood-Wu approach using a knock integral. Another neural network was trained to produce the necessary autoignition delay time of methanol mixtures, as calculated from detailed chemical kinetics.

These building blocks were then applied on two cases, one to check the feasibility of a 256 mm bore medium speed PFI SI methanol engine. The difficulty in getting methanol evaporated in the intake air, so to make best use of its cooling potential, was shown to severely limit the achievable power density.

A second case was aimed at producing the power density and efficiency as a function of bore size, of PFI SI methanol engines. Such data can be used in Energy System Optimisation models, to check the role of methanol in power-to-methanol-to-power schemes.

An important takeaway for the modelling is that there is a strong need for more experimental data on larger bore methanol-fuelled SI engines.

Acknowledgements

This research received funding from FASTWATER, a project within Europe's Horizon 2020 Research and Innovation program (Contract No.: 860251), BEST (Belgian Energy System) – a project funded by the Belgian federal Energy Transition Fund, and CHyPS (Chean Hydrogen-based Propulsion for Ships), funded by the Flemish Agency for Innovation and Entrepreneurship (VLAIO).

Literature

[1] S Verhelst, JWG Turner, L Sileghem, J Vancoillie. Methanol as a fuel for internal combustion engines. Progress in Energy and Combustion Science 70(2019):43–88, https://doi.org/10.1016/j.pecs.2018.10.001

[2] E Anetjärvi, E Vakkilainen, K Melin. Benefits of hybrid production of e-methanol in connection with biomass gasification. Energy 276(2023):127202, https://doi.org/10.1016/j.energy.2023.127202

[3] PF Flynn et al. Diesel Combustion: An Integrated View Combining Laser Diagnostics, Chemical Kinetics, And Empirical Validation. SAE Technical paper nr. 1999-01-0509, https://doi.org/10.4271/1999-01-0509

[4] M Svensson, M Tuner, S Verhelst. Investigation of Combustion Characteristics of a Fuel Blend Consisting of Methanol and Ignition Improver, Compared to Diesel Fuel and Pure Methanol. SAE Technical Paper nr. 2024-01-2122, https://doi.org/10.4271/2024-01-2122

[5] M Svensson, M Tuner, S Verhelst. Experimental Investigation of Pilot Injection Strategies to Aid Low Load Compression Ignition of Neat Methanol. SAE Technical Paper nr. 2024-01-2119, https://doi.org/10.4271/2024-01-2119

[6] M Svensson. Assessing single-fuel solutions enabling compression ignition of renewable methanol. PhD thesis, Lund University, 2024, https://portal.research.lu.se/en/publications/assessing-single-fuel-solutions-enabling-compression-ignition-of-

[7] CE Douglas. The Secret Horsepower Race – Western Front Fighter Engine Development. Tempest Books, 2022.

[8] K Ludvigsen. Classic Racing Engines: Expert Technical Analysis of Fifty of the Greatest Motorsports Power Units: 1913-1994. Bentley Publishers, 2017.

[9] Annex Report Number 56 Methanol as Motor Fuel, Appendices. A Report from the Advanced Motor Fuels Technology Collaboration, International Energy Agency, https://www.iea-amf.org/app/webroot/files/file/Annex%20Reports/AMF_Annex_56_Appendices.pdf

[10] Y-H Pu, D Dejaegere, M Svensson, S Verhelst. Renewable methanol as a fuel for heavy-duty engines : a review of technologies enabling single-fuel solutions. ENERGIES 2024, 17(7):1719, https://doi.org/10.3390/en17071719

[11] W Suijs, S Verhelst S. Scaling performance parameters of reciprocating engines for sustainable energy system optimization modelling. ENERGIES 2023, 16(22):7497. https://doi.org/10.3390/en16227497

[12] Y-H Pu, T Larsson, T Robeyn, M De Paepe, S Verhelst. Methanol evaporation in an engine intake runner under various conditions. SAE Technical Paper nr. 2023-24-0018, https://doi.org/10.4271/2023-24-0018

[13] B Abramzon, WA Sirignano. Droplet vaporization model for spray combustion calculations. International Journal of Heat and Mass Transfer, 32(9):1605–1618, 1989, https://doi.org/10.1016/0017-9310(89)90043-4

[14] AP Pinheiro, JM Vedovoto. Evaluation of droplet evaporation models and the incorporation of natural convection effects. Flow, Turbulence and Combustion, 102:537–558, 2019, https://doi.org/10.1007/s10494-018-9973-8

[15] J Welty, GL Rorrer, DG Foster. Fundamentals of momentum, heat, and mass transfer. John Wiley & Sons, 4th edition, 2001.

[16] GM Harpole. Droplet evaporation in high temperature environments. J. Heat Transfer. Feb 1981, 103(1): 86-91, https://doi.org/10.1115/1.3244437

[17] P Linstrom, W Mallard, editors. NIST Chemistry WebBook, NIST Standard Reference Database Number 69. National Institute of Standards and Technology, Accessed: 2024-04-06.

[18] CR Wilke. A viscosity equation for gas mixtures. Journal of Chemical Physics, 18(4):517–519, 1950.

[19] Y-H Pu, J Dierickx, S Verhelst, Modelling the evaporative cooling effect from methanol injection in the intake of internal combustion engines. Fuel 372(2024):132131, https://doi.org/10.1016/j.fuel.2024.132131

[20] SK Mahendar, T Larsson, AC Erlandsson. Alcohol lean burn in heavy duty engines: Achieving 25 bar IMEP with high efficiency in spark ignited operation. International Journal of Engine Research. 2021;22(11):3313-3324. https://doi.org/10.1177/1468087420972897

[21] A Güdden, S Pischinger, J Geiger, B Heuser, M Müther. An experimental study on methanol as a fuel in large bore high speed engine applications—Port fuel injected spark ignited combustion. Fuel 303(2021):121292, https://doi.org/10.1016/j.fuel.2021.121292

[22] W Suijs, Scaling the performance of methanol-fuelled spark ignition engines, PhD thesis, Ghent University, 2024, http://hdl.handle.net/1854/LU-01J0TH1XXCRCRWGQ5WEV7FZ0XR

[23] SS Alam, SW Rosa, C Depcik, SP Burugupally, E McDaniel, JD Hobeck. Modification of the Wiebe function for methane-air and oxymethane-based spark-ignition engines. Fuel 303(2021):121218, https://doi.org/10.1016/j.fuel.2021.121218

[24] N Blizard, J Keck. Experimental and theoretical investigation of turbulent burning model for internal combustion engines. SAE Technical Paper nr. 740191, 1974.

[25] M Metghalchi, JC Keck. Burning velocities of mixtures of air with methanol, isooctane, and indolene at high pressure and temperature. Combustion and flame, 48:191–210, 1982.

[26] J Vancoillie, S Verhelst, J Demuynck. Laminar burning velocity correlations for methanol-air and ethanol-air mixtures valid at SI engine conditions. SAE Technical Paper 2011-01-0846, https://doi.org/10.4271/2011-01-0846

[27] Introduction to Chem1d. https://github.com/thijsa93400/TUe_chem1d/wiki. Accessed: 2024-05-03.

[28] J Li, Z Zhao, A Kazakov, M Chaos, FL Dryer, JJ Scire Jr. A comprehensive kinetic mechanism for CO, CH2O, and CH3OH combustion. International Journal of Chemical Kinetics, 39(3):109–136, 2007, https://doi.org/10.1002/kin.20218

[29] S. K. Mahendar, A. C. Erlandsson. Semi-predictive modeling of diluted ethanol and methanol combustion in conventional spark ignition operation. SAE Technical Paper 2021-01-0386, https://doi.org/10.4271/2021-01-0386

[30] W. Suijs, J. Dierickx, Y.-H. Pu, Y. Wang, S. Verhelst. Calibrating the Livengood-Wu integral knock model for differently sized methanol engines. Fuel Communications, page 100121, 2024, https://doi.org/10.1016/j.jfueco.2024.100121

[31] S Shahpouri, et al. Laminar Flame Speed modeling for Low Carbon Fuels using methods of Machine Learning. Fuel, 333:126187, 2023, https://doi.org/10.1016/j.fuel.2022.126187

[32] C Pichler, EJ Nilsson. Reduced kinetic mechanism for methanol combustion in spark-ignition engines. Energy & fuels, 32(12):12805–12813, 2018, https://doi.org/10.1021/acs.energyfuels.8b02136

[33] J Vancoillie, L Sileghem, S Verhelst. Development and validation of a quasi-dimensional model for methanol and ethanol fueled SI engines. Applied Energy, 132:412–425, 2014, https://doi.org/10.1016/j.apenergy.2014.07.046

[34] A Lipatnikov, J Chomiak. Turbulent flame speed and thickness: phenomenology, evaluation, and application in multi-dimensional simulations. Progress in Energy and Combustion Science, 28(1):1–74, 2002, https://doi.org/10.1016/S0360-1285(01)00007-7

[35] J Livengood, P Wu. Correlation of autoignition phenomena in internal combustion engines and rapid compression machines. Symposium (International) on Combustion, 5:347–356, 1955

[36] https://www.cantera.org/. Accessed: 2024-05-03.

[37] FASTWATER: FAST Track to Clean and Carbon-Neutral WATERborne Transport. EU H2020 project Contract Nr. 860251, https://fastwater.eu/

[38] BEST: Belgian Energy System project, https://uclouvain.be/en/research-institutes/immc/belgian-energy-system-%26ndash%3B-best-2020-2024.html

[39] Y-H Pu, W Suijs, R De Graeve, S Verhelst. Evaluation of a virtual medium-speed engine on methanol using spark-ignition. CIMAC 2023 : 30th CIMAC World Congress, Proceedings, paper 012.

[40] A. Sorrentino, V. Leytes, L. Mattheeuws, E. D. Wilde. Methanol port fuel injection for medium-speed application: injector development and engine design. In Proceedings of 30th CIMAC World Congress, 2023

[41] J. B. Heywood. Internal Combustion Engine Fundamentals, McGraw-Hill series in mechanical engineering. 1988.